

Title	Coastal iodine emissions: part 2. Chamber experiments of particle formation from Laminaria digitata-derived and laboratory-generated I ₂
Authors	Monahan, Ciaran;Ashu-Ayem, Enowmbi R.;Nitschke, Udo;Darby, Steven B.;Smith, Paul D.;Stengel, Dagmar B.;Venables, Dean S.;O'Dowd, Colin D.
Publication date	2012
Original Citation	MONAHAN, C., ASHU-AYEM, E. R., NITSCHKE, U., DARBY, S. B., SMITH, P. D., STENGEL, D. B., VENABLES, D. S. & O'DOWD, C. D. 2012. Coastal Iodine Emissions: Part 2. Chamber Experiments of Particle Formation from Laminaria digitata-Derived and Laboratory-Generated I ₂ . Environmental Science & Technology, 46, 10422-10428. doi: 10.1021/es3011805
Type of publication	Article (peer-reviewed)
Link to publisher's version	10.1021/es3011805
Rights	Copyright © 2012 American Chemical Society. This document is the Accepted Manuscript version of a Published Work that appeared in final form in Environmental Science and Technology, copyright © American Chemical Society after peer review and technical editing by the publisher. To access the final edited and published work see http://pubs.acs.org/doi/abs/10.1021/es3011805
Download date	2024-05-02 21:57:22
Item downloaded from	https://hdl.handle.net/10468/788



UCC

University College Cork, Ireland
Coláiste na hOllscoile Corcaigh

**Coastal Iodine Emissions:
Part 2. Chamber Experiments
into Particle Formation from
Laminaria digitata-Derived
and Laboratory-Generated I₂**

Journal:	<i>Environmental Science & Technology</i>
Manuscript ID:	Draft
Manuscript Type:	Article
Date Submitted by the Author:	n/a
Complete List of Authors:	monahan, ciaran; NUIG, Physics Ashu-Ayem, Tina; UCC, Chemistry Nitschke, Udo; NUIG, SoNS Derby, Steven; UCC, Chemistry Smith, Paul; UCC, Chemistry Stengal, Dagmar; NUIG, SoNS Venables, Dean; University of College Cork, Chemistry o'Dowd, Colin; NUIG, Physics

SCHOLARONE™
Manuscripts

1
2
3
4
5
6
7
8
9
10
11
12
13
14
15
16
17
18
19
20
21
22
23
24
25
26
27
28
29
30
31
32
33
34
35
36
37
38
39
40
41
42
43
44
45
46
47
48
49
50
51
52
53
54
55
56
57
58
59
60

Coastal Iodine Emissions: Part 2. Chamber Experiments into Particle Formation from *Laminaria digitata*-Derived and Laboratory-Generated I₂

CIARAN MONAHAN¹, ENOWMBI R. ASHU-AYEM², UDO NITSCHKE³,
STEVEN B. DARBY², PAUL D. SMITH², DAGMAR B. STENGEL³, DEAN S.
VENABLES² AND COLIN D. O'DOWD^{1*}

¹*School of Physics and Centre for Climate & Air Pollution Studies, Ryan Institute, National University of Ireland Galway, Galway, Ireland,* ²*Department of Chemistry and Environmental Research Institute, University College Cork, Cork, Ireland,* and ³*Botany and Plant Science, School of Natural Sciences and Ryan Institute, National University of Ireland Galway, Galway, Ireland*

Received 2012, Revised manuscript received 2012. Accepted, 2012

1
2
3 Laboratory studies into particle formation from *L. digitata* macroalgae were
4 undertaken to elucidate aerosol formation for a range of I₂ (0.3-76 ppb_v) and O₃ (<3-
5 96 ppb_v) mixing ratios and light-levels ($E_{PAR} = 15-235 \mu\text{mol photons m}^{-2} \text{s}^{-1}$). No clear
6 pattern was observed for I₂ or aerosol parameters as a function of light-levels;
7 however, aerosol mass fluxes (assuming I₂O₄ gas-to-particle conversion) and particle
8 number concentrations were correlated ($R^2=0.7$ and 0.95 , respectively) with I₂ mixing
9 ratios for low O₃ mixing ratios (<3 ppb_v). Additional experiments into particle
10 production as a function of laboratory-generated I₂, over a mixing ratio range of 1-8
11 ppb_v, were conducted under moderate O₃ mixing ratios (~24 ppb_v) where a clear, 100-
12 fold or greater, increase in the aerosol number concentrations and mass fluxes was
13 observed compared to the low-O₃ experiments. A linear relationship between particle
14 concentration and I₂ was found, in reasonable agreement with previous studies.
15 Scaling the laboratory relationship to aerosol concentrations typical of the coastal
16 boundary layer suggests a I₂ mixing ratio range of 6-93 ppt_v can account for the
17 observed particle production events. Aerosol number concentration produced from I₂
18 is more than a factor of 10 higher than that produced from CH₂I₂ for the same mixing
19 ratios.
20
21
22
23
24
25
26
27
28
29
30
31
32
33
34
35
36
37
38
39
40
41
42
43
44
45
46
47
48
49
50
51
52
53
54
55
56
57
58
59
60

Introduction

The release of volatile iodine organic compounds and of molecular iodine (I_2) into the marine boundary layer (MBL) has been linked to the rapid production of large numbers of new, ultrafine, aerosol particles¹⁻⁴. The nucleation and growth events have been observed to occur most frequently in coastal areas under conditions of solar irradiation and low tide. Initial studies on the dominant aerosol precursor focused on the release of CH_2I_2 by shore biota^{2, 5, 6}; however, it was later shown that the dominant iodine source is more likely to be I_2 ^{7, 8}. In fact, *McFiggans*. (2004)⁷ found that the iodine flux from I_2 was three orders of magnitude higher than that from CH_2I_2 , due to a higher photolysis rate for I_2 . Photo-chemically produced iodine atoms react rapidly with ozone to produce iodine monoxide radicals (IO) which subsequently self-react to form iodine dioxide radicals (OIO) and I_2O_4 . A fraction of the newly formed I_2O_4 may then form new particles while reaction with IO may form I_2O_3 which again may react with O_3 to form I_2O_5 ^{7, 9-11}. Modelling studies have also suggested that OIO or I_xO_y molecules may co-nucleate or co-condense with other molecules such as H_2SO_4 and/or low-volatility organic compounds^{12, 13}. Most previous laboratory studies have focused on the common kelp *Laminaria (L.) digitata* which is prone to high I_2 emission rates when exposed to oxidative stresses^{14,15,16, 17,18,19}. Field-chamber experiments (using scrubbed marine air) have shown a linear correlation between new particle formation and I_2 mixing ratios from *Laminaria* and *Fucus* species²⁰ in the vicinity of Mace Head, located on the Irish – Atlantic coastline²¹. This work extends previous studies^{22,23,24} into particle production from I_2 emissions from a number of different seaweed species in that it specifically focuses on aerosol formation for a wide range of I_2 mixing ratios from a strong I_2 emitter, *L. digitata*, under a wider range of conditions (i.e. various light levels and ozone mixing

1
2
3 ratios), followed by the quantification of aerosol production from laboratory-
4
5 generated I₂, for moderate ozone mixing ratios.
6
7
8
9

10 This report comprises Part 2 of a two-part study – Part 1 focuses on I₂ emission rates
11
12 from *L. digitata* under various environmental conditions and is reported in *Ashu-Ayem*
13
14 *et al.*, (2012).
15
16
17
18
19
20
21

22 **Experimental Section**

23
24 Experiments were carried out in an atmosphere simulation chamber comprising a
25
26 cylindrical FEP bag housed inside a 2 m long enclosure. The chamber volume was
27
28 2.2 m³ and its surface area was approximately 10 m². A photolysis light source,
29
30 comprising an externally-mounted 2 kW xenon lamp (Rige Lighting), produced a
31
32 circular collimated beam above the chamber. The lamp spectrum (400 to 850 nm,
33
34 $\lambda_{\text{max}} = 550$ nm) provided simulated Photosynthetically Active Radiation (PAR)
35
36 spectrum leading to an I₂ chamber photolysis rate of 0.0075±0.0010 s⁻¹. Ozone was
37
38 added using an Ozone Lab model OL80W/FM ozone generator. An incoherent
39
40 broadband cavity-enhanced absorption spectroscopy (IBBCEAS) system was the
41
42 principle tool for analyzing the gas phase composition of the chamber^{26,27}. The
43
44 IBBCEAS comprised two optical cavities across the length of the chamber: a blue
45
46 channel (420 to 460 nm) for IO and a green channel (520 to 560 nm) for I₂ and OIO.
47
48 Reference spectra for IO and OIO were obtained from *Spietz et al.* and *Bloss et al.*
49
50 respectively, and convoluted to this particular instrument function^{28,29}. O₃ was
51
52 monitored using a UV absorption monitor (2B Technologies model 202) with a
53
54 sampling rate of 1 L min⁻¹.
55
56
57
58
59
60

1
2
3
4
5
6 A nano scanning mobility particle sizer (n-SMPS), comprising a Thermo Systems Inc.
7 (TSI) model 3776 condensation particle counter with a TSI model 3085 differential
8 mobility analyzer, was operated continuously to measure particle sizes from 3nm to
9 20nm while a TSI model 3034 scanning mobility particle sizer (SMPS) was used in
10 conjunction with the n-SMPS to measure particle size ranges a further 20 nm – 500
11 nm. The SMPS was only available for the third set of experiments. The n-SMPS and
12 SMPS were operated with a time resolution of 20 s and 120 s respectively.
13
14
15
16
17
18
19
20
21

22 Repeated measurements in the chamber in the absence of *L. digitata* showed zero or
23 close to zero particles, zero I₂, and levels of O₃ around the detection level of the
24 instrument. Two types of static experiments were conducted on *L. digitata*: (1) iodine
25 emission and subsequent particle formation from five replicas were examined under
26 “low” (15 μmol photons m⁻² s⁻¹), “medium” (100 μmol photons m⁻² s⁻¹) and “high”
27 (235 μmol photons m⁻² s⁻¹) irradiances and under very ozone mixing ratios (< 3 ppb_v);
28 and (2) iodine emissions and particle formation under low (15 μmol photons m⁻² s⁻¹)
29 irradiances but with ozone mixing ratios of the order of ~94 ppb_v. It should be noted
30 that “high” light conditions here corresponds to 15% of the upper light limit that algae
31 would be exposed to under real-world conditions. A third set of experiments were
32 conducted on a range of mixing ratios of laboratory-generated I₂ under flow-through
33 conditions and ozone mixing ratios ~24 ppb_v. For the *L. digitata* experiments, algae
34 were placed in a 33 L tray filled with natural seawater which and were allowed to
35 acclimatise over 10 minutes afterwhich the seawater was gradually drained over the
36 following 10 minutes (i.e. to mimic an outgoing tide). A complete description of
37 experimental methodologies can be found in *Ashu-Ayem et al.*, (2012)
38
39
40
41
42
43
44
45
46
47
48
49
50
51
52
53
54
55
56
57
58
59
60

Results & Discussion

Particle Formation Under Different Light Conditions and Low O₃. *L. digitata* samples were exposed to irradiances of E_{PAR} = 15, 100 and 235 $\mu\text{mol photons m}^{-2} \text{s}^{-1}$, labelled “low”, “medium” and “high” light conditions, respectively under static-chamber flow conditions. Experiments were performed at each light-level using five replicate *L. digitata* specimens to account for potential high variability in I₂ emission rates as previously observed²³ (See Table 1 in *Ashu-Ayem et al.*, (2012), and Supplementary Information for full experimental summary).

Particle formation was observed in all experiments when exposed to light and low-O₃ air. A characteristic strong particle burst, ~10-30 s after the start of the experiment, and peaking at concentrations ranging from $2.6 \times 10^4 \text{ cm}^{-3}$ - $3.9 \times 10^7 \text{ cm}^{-3}$, corresponding to a range I₂ mixing ratios from 5.3 – 76.3 ppb_v, was observed. Figure 1 illustrates the evolution of the aerosol size distribution, O₃, I₂, and IO mixing ratios, the aerosol condensation mass flux (determined by the increase in nSMPS-derived volume, taking an I₂O₄ density of 2.5 g cm^{-3}), and number concentration. For medium light levels, I₂ mixing ratios of 1.1 - 20.2 ppb_v led to particle concentrations of $7 \times 10^3 \text{ cm}^{-3}$ - $3.9 \times 10^6 \text{ cm}^{-3}$, while for high light levels, particle concentration ranged from $2.1 \times 10^6 \text{ cm}^{-3}$ - $3.8 \times 10^7 \text{ cm}^{-3}$ for I₂ mixing ratios of 4.1-36.8 ppb_v. The condensable mass flux for the low, medium and high light-level experiments ranged from $2.4 \times 10^{-10} \mu\text{g cm}^{-3} \text{ s}^{-1}$ - $1.7 \times 10^{-7} \mu\text{g cm}^{-3} \text{ s}^{-1}$, $2.3 \times 10^{-10} \mu\text{g cm}^{-3} \text{ s}^{-1}$ - $1.7 \times 10^{-8} \mu\text{g cm}^{-3} \text{ s}^{-1}$ and $2.5 \times 10^{-9} \mu\text{g cm}^{-3} \text{ s}^{-1}$ - $5.3 \times 10^{-7} \mu\text{g cm}^{-3} \text{ s}^{-1}$, respectively. Full details are tabulated in Table S1 in Supplementary Material.

1
2
3 The experiments in this study did not reveal and clear pattern between biomass, light-
4 levels and either I₂ mixing ratios (as discussed in Part 1 of the study) or particle
5 concentration. However, for the low and medium light-level experiments, a high
6 correlation coefficient, fitted in log—log space, was found between mass flux and I₂
7 mixing ratio ($R^2=0.7$ and 0.95 , respectively). Similarly high correlations were found
8 for number concentration and I₂ mixing ratio ($R^2=0.83$ for low light-levels and 0.98
9 for medium light-levels). For the highest light-level, R^2 for mass flux as a function of
10 I₂ mixing ratio was -0.02 , in stark contrast to the low and medium light levels. From
11 the 5 high light-level replicates, two concurrent samples (#12 and #13) stand out in
12 that they are associated with relatively high biomass, quite low I₂ mixing ratios, and
13 the highest mass flux. Variability in I₂ emissions could explain the low I₂ mixing
14 ratios resulting from moderate to high amounts of biomass; however, the aerosol
15 condensation flux yield for the corresponding I₂ mixing ratios is 1-2 orders of
16 magnitude higher in these samples compared to all others (specifically, the ratio of
17 mass flux over I₂ mixing ratio for these two samples ranges from $2-8 \times 10^{-8} \mu\text{g cm}^{-3} \text{s}^{-1}$
18 ppb_v^{-1} while the ratio for the other samples ranges from 4×10^{-11} to $5 \times 10^{-9} \mu\text{g cm}^{-3}$
19 $\text{s}^{-1} \text{ppb}_v^{-1}$). Such ratios are equivalent to those observed in the later O₃ – rich
20 experiments.

21
22
23
24
25
26
27
28
29
30
31
32
33
34
35
36
37
38
39
40
41
42
43
44
45
46
47
48 It should be noted that the air in the chamber prior to each replicate had an O₃ mixing
49 ratio that was at or below detection limit of 3 ppb_v; however, particle formation still
50 proceeded. Therefore, O₃ was present in sufficient concentrations to produce
51 significant quantities of aerosol, although still at or below detection limits. It is
52 thought that either O₃ was produced by trace amounts of VOCs and NO_x entering the
53 chamber from laboratory air or direct entrainment of O₃ from laboratory air. We
54
55
56
57
58
59
60

1
2
3 suggest that samples #12 and # 13 were potentially influenced by slightly elevated O₃
4
5 mixing ratios resulting in significant increases in aerosol yield, thus also explaining
6
7 the low I₂ mixing ratios for relatively high biomass abundance. In fact, peak O₃
8
9 values recorded above the detection limit were 3-4 times higher for these two
10
11 particular cases compared to the other samples (even spiking at 18 ppb_v). In light of
12
13 the suspicion relating to comparability of the replicate #12 and #13 experiments in
14
15 terms of O₃ upper mixing ratios, we have removed these cases from further analysis.
16
17
18 The remaining three data lead to a $R^2=0.98$ for a log-log fit, indicating minimal scatter
19
20 across these remaining samples. The remaining low, medium and high light-level
21
22 datasets were grouped together, excluding sample #12 and #13, for an overall analysis
23
24 and the inter-relationships between mass flux and concentration, as a function of
25
26 mixing ratio, are shown in Figure 2. The mass flux versus I₂ mixing ratio exhibited a
27
28 correlation of $R^2=0.72$, while the number concentration exhibited a correlation of
29
30 $R^2=88$ with mixing ratio. Further investigations are required to address the
31
32 variability in I₂ emission rates from *L. digitata*, as discussed in more detail in Part 1,
33
34 *Ashu-Ayem et al.*, (2012).
35
36
37
38
39
40
41
42

43 **Particle Formation Under Low Light Conditions and High O₃.** An experiment
44
45 composed of five replicates (replicates #21 - #25 - See Table 2 in Part 1) was also
46
47 carried out. All algal specimens were of similar age and weight as those in the low
48
49 light - low O₃ experiment (see Table S.1) Experimental conditions were kept the
50
51 same as those of replicates #16 - #20 (i.e. low light) except for O₃ mixing ratios of 92-
52
53 96 ppb_v. As in the previous experiments under low O₃, mixing ratios, the resulting I₂
54
55 mixing ratio varied enormously from sample to sample with no correlation between
56
57 biomass being observed. This, in turn, led to variability in the characteristics of the
58
59
60

1
2
3 resultant aerosol number concentration and mass flux. For the general collection of
4 replicates, a higher rate of aerosol mass flux was observed under high O₃ conditions,
5 perhaps resulting from a combined O₃ influence on both increased I₂ emissions
6 resulting from potential oxidative stress of the algae along with increased particle
7 production through oxidation processes; however, it is not possible to distinguish
8 between the two processes since oxidative stress was not quantified in this
9 experimental set up.
10
11
12
13
14
15
16
17
18
19
20
21

22 A typical particle size distribution evolution associated with this experiment is shown
23 in Figure 3 where the experiment was observed to yield concentrations of particles of
24 $3.5 \times 10^7 \text{ cm}^{-3}$ associated with I₂ mixing ratios of 17 ppbv. In each of the replicates, an
25 initial peak was observed followed by a second and stronger peak shortly after a steep
26 rise in I₂ and IO mixing ratios. This can be seen in Figure 3, where the initial, and
27 less intense peak was observed at ~11:40 am and the subsequent, stronger, peak was
28 seen at ~12:10 pm. The maximum particle number concentration occurs at 4.2×10^7
29 cm^{-3} ; however, the true concentration is expected to be higher as the growth rate of
30 newly formed particles is so rapid that the mode diameter rapidly grows past the
31 upper diameter detection limit of the nSMPS.
32
33
34
35
36
37
38
39
40
41
42
43
44
45
46
47

48 The overall particle number concentration increased from between $1 \times 10^4 \text{ cm}^{-3}$ and 1
49 $\times 10^7 \text{ cm}^{-3}$ during the low ozone mixing ratio experiment to greater than $1 \times 10^7 \text{ cm}^{-3}$
50 during the high O₃ mixing ratio experiment, although due to the rapid modal growth
51 out of the measurement size range, no quantitative relationship can be derived. The
52 mass flux ranged from $8.2 \times 10^{-8} \mu\text{g cm}^{-3} \text{ s}^{-1}$ to $1.2 \times 10^{-6} \mu\text{g cm}^{-3} \text{ s}^{-1}$, compared to 2.3
53 $\times 10^{-10} \mu\text{g cm}^{-3} \text{ s}^{-1}$ to $1.7 \times 10^{-7} \mu\text{g cm}^{-3} \text{ s}^{-1}$ for a the low O₃, low light experiment.
54
55
56
57
58
59
60

1
2
3 This indicates at least 2 orders of magnitude more aerosol mass production in the
4 presence of abundant ozone mixing ratios.
5
6
7

8
9
10 The effects of exposure of *L. digitata* to O₃ and the subsequent enhancement in the
11 particle number concentration by several orders of magnitude have been reported in
12 previous studies^{9, 15, 17}; however, what remains unclear in these experiments is if
13 exposure to O₃ leads to an increased I₂ net production rates ($P > 0.05$; see Table 1 and
14 2 in Part 1) in experiments with higher O₃ mixing despite the specimens being in
15 similar light conditions (15 μmol photons m⁻² s⁻¹), although there is a trend of higher
16 net production rates if normalised to biomass weight. For this set of experiments,
17 there was no conclusive statistical link between particle number concentration and I₂
18 mixing ratios; however, particle concentrations were generally higher for the high
19 ozone mixing ratios. The lack of a statistical link, as suggested above, may be due to
20 the rapid growth of the nucleation mode out of the nSMPS detection range.
21
22
23
24
25
26
27
28
29
30
31
32
33
34
35
36
37

38 IO trends tracked generally that of I₂, however, mixing ratios were typically two
39 orders of magnitude lower. OIO, a by-product of the IO-IO self-reaction, is not
40 detected despite having been considered the main precursor of iodine oxide aerosol
41 particles. The interactions between I₂, IO and OIO are discussed in Part 1 of the study
42 where the lack of detectable OIO (detection limit 30 ppt_v) is attributed to fast
43 reactions between OIO and I atoms under the mixing ratio conditions in the chamber.
44
45
46
47
48
49
50
51
52
53
54

55 **Particle Production as a Function of I₂ Mixing Ratio.** In order to further study the
56 role of I₂ in particle formation, a set of experiments were conducted under laboratory
57 generated and controlled I₂ mixing ratios and a moderate O₃ mixing ratio of 24 ppb_v,
58
59
60

1
2
3 regarded as representative of tropospheric conditions ³⁰. The experiments were
4 carried out with a “flow through” configuration of 225 L min⁻¹ applied to the chamber
5 where light intensity was fixed at 100 μmol photons m⁻² s⁻¹ and I₂ mixing ratios varied
6 from 1 ppb_v to 8 ppb_v (see Table 1). The flow-through experiment did not comprise
7 continuous supply of O₃ and I₂, more so, O₃ concentrations were set to 24 ppb_v in the
8 chamber and then a pulse of I₂ was introduced. Controlled I₂ mixing ratios were
9 generated by evaporating I₂-methanol solutions of known concentrations to dryness,
10 followed by heating the I₂ residue in a stream of nitrogen into the chamber.
11
12
13
14
15
16
17
18
19
20
21
22

23 In each experiment, on mixing I₂ and O₃ in the photolysis chamber, both mixing ratios
24 were rapidly reduced due to combined photolysis, oxidation and subsequent formation
25 and growth of the aerosol. For each replicate the total particle number concentration
26 increased rapidly initially, reaching its peak after about 10 minutes from the inception
27 of photolysis and then rapidly decayed. Figure 4 illustrates the general evolution of
28 the aerosol number concentrations in relation to the gas species mixing ratios over
29 time. For the example shown in Figure 4, the initial ozone mixing ratio was 24
30 ppb_v, and after the introduction of I₂ into the chamber, I₂ peaked at 6.6 ppb_v while
31 simultaneously IO peaked at 0.1 ppb_v. tens of seconds later, particle production was
32 observed and after about five minutes, a peak concentration of 9 x 10⁷ cm⁻³ was
33 observed. By the time the peak aerosol concentration was observed, both I₂ and IO
34 mixing ratios had reduced by a factor of 2. I₂ decayed more rapidly than IO. For the
35 other experiments, I₂ ranged from 1.0 ppb_v to 8.1 ppb_v and the total aerosol
36 concentration ranged from 2.5×10⁶ cm⁻³ to 1.1×10⁸ cm⁻³, respectively, while 3 nm
37 particle concentration ranged from 8.9 ×10⁴ cm⁻³ to 3.7 ×10⁶ cm⁻³, respectively.
38
39
40
41
42
43
44
45
46
47
48
49
50
51
52
53
54
55
56
57
58

59 Comparison of the condensing mass flux and number concentration, over the range of
60 I₂ mixing ratios overlapping (i.e. 1-8 ppb_v) in the low ozone experiment and the

1
2
3 moderate ozone experiment, illustrates generally 2-3 orders of magnitude greater
4 mass flux in the moderate ozone experiment (see Figure 5).
5
6

7
8 The total particle number concentration, as well as the 3 nm particle concentration
9 increased linearly as the initial I₂ mixing ratio was increased. The linear fit (in linear
10 space) between I₂ and total particle concentration is shown in Figure 4 and was found
11 to be $N_{tot} (cm^{-3}) = 1.34 \times 10^7 I_2 (ppb_v)$ while the linear fit between 3 nm particle
12 concentration and I₂ was found to be $N_{3nm} (cm^{-3}) = 4.69 \times 10^5 I_2 (ppb_v)$. The total
13 particle concentration as a function of IO was also seen to increase linearly with
14 increasing IO.
15
16
17
18
19
20
21
22
23
24
25
26

27 The correlations between I₂ and particle concentrations, shown in Figure 6, were
28 $R^2=0.7$ for both the total and 3 nm particle concentrations, with more scatter having
29 been observed for lower values of I₂. During the course of the present study, other
30 species such as HOI may have been preferentially formed at different mixing ratios
31 but not detectable by IBBCEAS methods and may contribute a “missing” component
32 in the cycle. The relationship between particle concentration and I₂ in this study is
33 compared to that from *Sellegri et al.*, (2005), extending up to 400 ppt_v, along with the
34 relationship between particle concentration and CH₂I₂ mixing ratios reported by
35 *Burkholder et al.*, (2004) and *Jimenez et al.*, (2003). While the I₂ mixing ratios in this
36 study are higher than *Sellegri et al.* comparison of both relationships indicates a
37 greater particle concentration generated by *Sellegri et al.* at low I₂ mixing ratios, but
38 relatively similar concentrations at high I₂ mixing ratios. Both this study and that of
39 *Sellegri et al.* illustrate at least an order of magnitude higher aerosol yield from I₂
40 compared to that from CH₂I₂, consistent with differences in photolysis lifetimes.
41
42
43
44
45
46
47
48
49
50
51
52
53
54
55
56
57
58
59
60

1
2
3 **Comparison to Ambient Measurements.** Results arising from the flow-through
4 chamber studies reported here can be directly compared to field measurements of
5 coastal, iodine-driven, new particle production events^{2, 31}. While the concentrations
6 in the laboratory are significantly higher than observed in the field, they can be
7 extrapolated down to lower concentrations in order to estimate the I₂ mixing ratios
8 required to produce observed particles in coastal events such as those at Mace Head.
9
10 Over the period from 1st May 2010 to the 1st August 2010, 28 typical clean air
11 coastal production events were analysed and were found to have a total particle
12 concentration range between $7.8 \times 10^4 \text{ cm}^{-3}$ - $1.2 \times 10^6 \text{ cm}^{-3}$ and a peak 3 nm particle
13 concentration range of $4.3 \times 10^3 \text{ cm}^{-3}$ - $9.4 \times 10^4 \text{ cm}^{-3}$. Scaling the relationships
14 between particle concentration and I₂ downward to observed concentrations in the
15 field points to a coastal boundary layer I₂ mixing ratio of 6-93 ppt_v. Values in this
16 range are in line with a previous studies by *Saiz-Lopez and Plane* (2004) who found
17 that the nucleation events observed at Mace Head ($N_{3nm} = 5 \times 10^4 \text{ cm}^{-3}$) could be
18 produced by the daytime photolysis of 10 ppt_v I₂, typical of the daytime mixing ratios
19 observed at low tide during the measurement period.
20
21
22
23
24
25
26
27
28
29
30
31
32
33
34
35
36
37
38
39
40
41
42
43

44 **ACKNOWLEDGMENT**

45
46
47 We thank Science Foundation Ireland for supporting this research through grants
48 07/RFP/GEOF716 and 09/RFP/CAP2509. UN gratefully appreciates financial support
49 through the Irish Research Council for Science, Engineering and Technology
50 (IRCSET “Embark Initiative”). COD and CM also acknowledge EC funding under
51 the MAP and EUCAARI and EUSAAR.
52
53
54
55
56
57
58
59
60

References

1. McFiggans, G.; Bale, C. S. E.; Ball, S. M.; Beames, J. M.; Bloss, W. J.; Carpenter, L. J.; Dorsey, J.; Dunk, R.; Flynn, M. J.; Furneaux, K. L.; Gallagher, M. W.; Heard, D. E.; Hollingsworth, A. M.; Hornsby, K.; Ingham, T.; Jones, C. E.; Jones, R. L.; Kramer, L. J.; Langridge, J. M.; Leblanc, C.; LeCrane, J. P.; Lee, J. D.; Leigh, R. J.; Longley, I.; Mahajan, A. S.; Monks, P. S.; Oetjen, H.; Orr-Ewing, A. J.; Plane, J. M. C.; Potin, P.; Shillings, A. J. L.; Thomas, F.; von Glasow, R.; Wada, R.; Whalley, L. K.; Whitehead, J. D., Iodine-mediated coastal particle formation: an overview of the Reactive Halogens in the Marine Boundary Layer (RHAMBLE) Roscoff coastal study. *Atmos. Chem. Phys.* **2010**, 10, (6), 2975-2999.
2. O'Dowd, C. D.; Jimenez, J. L.; Bahreini, R.; Flagan, R. C.; Seinfeld, J. H.; Hameri, K.; Pirjola, L.; Kulmala, M.; Jennings, S. G.; Hoffmann, T., Marine aerosol formation from biogenic iodine emissions. *Nature* **2002**, 417, (6889), 632-636.
3. Saiz-Lopez, A.; Shillito, J. A.; Coe, H.; Plane, J. M. C., Measurements and modelling of I₂, IO, OIO, BrO and NO₃ in the mid-latitude marine boundary layer. *Atmos. Chem. Phys.* **2006**, 6, (6), 1513-1528.
4. Whitehead, J. D.; McFiggans, G. B.; Gallagher, M. W.; Flynn, M. J., Direct linkage between tidally driven coastal ozone deposition fluxes, particle emission fluxes, and subsequent CCN formation. *Geophys. Res. Lett.* **2009**, 36, (4), L04806.
5. Hoffmann, T.; O'Dowd, C. D.; Seinfeld, J. H., Iodine oxide homogeneous nucleation: An explanation for coastal new particle production. *Geophys. Res. Lett.* **2001**, 28, (10), 1949-1952.
6. Jimenez, J. L.; Bahreini, R.; Cocker, D. R., III; Zhuang, H.; Varutbangkul, V.; Flagan, R. C.; Seinfeld, J. H.; O'Dowd, C. D.; Hoffmann, T., New particle formation from photooxidation of diiodomethane (CH₂I₂). *J. Geophys. Res.* **2003**, 108, (D10), 4318.
7. McFiggans, G.; Coe, H.; Burgess, R.; Allan, J.; Cubison, M.; Rami Alfarra, M.; Saunders, R.; Saiz-Lopez, A.; Plane, J. M. C.; Wevill, D.; Carpenter, L.; Rickard, A. R.; Monks, P. S., Direct evidence for coastal iodine particles from *Laminaria* macroalgae; linkage to emissions of molecular iodine. *Atmos. Chem. Phys. Discuss.* **2004**, 4, (1), 939-967.
8. Saiz-Lopez, A.; Plane, J. M. C., Novel iodine chemistry in the marine boundary layer. *Geophys. Res. Lett.* **2004**, 31, (4), L04112.
9. Burkholder, J. B.; Curtius, J.; Ravishankara, A. R.; Lovejoy, E. R., Laboratory studies of the homogeneous nucleation of iodine oxides. *Atmos. Chem. Phys.* **2004**, 4, (1), 19-34.
10. Kaltsoyannis, N.; Plane, J. M. C., Quantum chemical calculations on a selection of iodine-containing species (IO, OIO, INO₃, (IO)₂, I₂O₃, I₂O₄ and I₂O₅) of importance in the atmosphere. *Physical Chemistry Chemical Physics* **2008**, 10, (13), 1723-1733.
11. Pirjola, L.; O'Dowd, C.; Yoon, Y. J.; Sellegri, K., Modelling Iodine Particle Formation and Growth from Seaweed in a Chamber. *Environmental Chemistry* **2005**, 2, (4), 271-281.
12. Ciaran Monahan, Henri Vuollekoski, Markku Kulmala, and Colin O'Dowd, "Simulating Marine New Particle Formation and Growth Using the M7 Modal Aerosol Dynamics Modal," *Advances in Meteorology*, vol. 2010, Article ID 689763, 9 pages, **2010**.

- 1
2
3
4
5
6
7
8
9
10
11
12
13
14
15
16
17
18
19
20
21
22
23
24
25
26
27
28
29
30
31
32
33
34
35
36
37
38
39
40
41
42
43
44
45
46
47
48
49
50
51
52
53
54
55
56
57
58
59
60
13. Vuollekoski, H.; Kerminen, V. M.; Anttila, T.; Sihto, S. L.; Vana, M.; Ehn, M.; Korhonen, H.; McFiggans, G.; O'Dowd, C. D.; Kulmala, M., Iodine dioxide nucleation simulations in coastal and remote marine environments. *J. Geophys. Res.* **2009**, 114, (D2), D02206.
 14. Kupper, F. C.; Carpenter, L. J.; Gordon, B. M.; Palmer, C. J.; Waite, T. J.; Boneberg, E.-M.; Woitsch, S.; Weiller, M.; Abela, R.; Grolimund, D.; Potin, P.; Alison, B.; Luther, G. W., III; Kroneck, P. M. H.; Meyer-Klaucke, W.; Feitersm, M. C., Iodide Accumulation Provides Kelp with an Inorganic Antioxidant Impacting Atmospheric Chemistry. *Proceedings of the National Academy of Sciences of the United States of America* **2008**, 105, (19), 6954-6958.
 15. Palmer, C. J.; Anders, T. L.; Carpenter, L. J.; Kupper, F. C.; McFiggans, G. B., Iodine and Halocarbon Response of *Laminaria digitata* to Oxidative Stress and Links to Atmospheric New Particle Production. *Environmental Chemistry* **2005**, 2, (4), 282-290.
 16. Bale, C.; Ingham, T.; Commane, R.; Heard, D.; Bloss, W., Novel measurements of atmospheric iodine species by resonance fluorescence. *Journal of Atmospheric Chemistry* **2008**, 60, (1), 51-70.
 17. Dixneuf, S.; Ruth, A. A.; Vaughan, S.; Varma, R. M.; Orphal, J., The time dependence of molecular iodine emission from *Laminaria digitata*. *Atmos. Chem. Phys.* **2009**, 9, (3), 823-829.
 18. Nitschke, U.; Ruth, A.; Dixneuf, S.; Stengel, D., Molecular iodine net production rates and photosynthetic performance of different thallus parts of *Laminaria digitata*; (Phaeophyceae) during emersion. *Planta* **2011**, 233, (4), 737-748.
 19. Kundel, M.; Thorenz, U.; Petersen, J.; Huang, R.-J.; Bings, N.; Hoffmann, T., Application of mass spectrometric techniques for the trace analysis of short-lived iodine-containing volatiles emitted by seaweed. *Analytical and Bioanalytical Chemistry* **2012**, 402, (10), 3345-3357.
 20. Sellegri, K.; Yoon, Y. J.; Jennings, S. G.; O'Dowd, C. D.; Pirjola, L.; Cautenet, S.; Chen, H.; Hoffmann, T., Quantification of Coastal New Ultra-Fine Particles Formation from In situ and Chamber Measurements during the BIOFLUX Campaign. *Environmental Chemistry* **2005**, 2, (4), 260-270.
 21. O'Connor, T.C., S.G. Jennings, and C.D. O'Dowd, Highlights from 50 years of Aerosol Measurements at Mace Head, *Atmos. Res.*, 90, 338-355, doi:10.1016/j.atmosres.2008.08.014, **2008**.
 22. Ball, S. M.; Hollingsworth, A. M.; Humbles, J.; Leblanc, C.; Potin, P.; McFiggans, G., Spectroscopic studies of molecular iodine emitted into the gas phase by seaweed. *Atmos. Chem. Phys.* **2010**, 10, (13), 6237-6254.
 23. Huang, R. J., Seitz, K., Neary, T., O'Dowd, C. D., Platt, U., Hoffmann T., Observations of high concentrations of I₂ and IO in coastal air supporting iodine-oxide driven coastal new particle formation, *Geophys. Res. Lett.*, **2010**, 37, L03803, doi:10.1029/2009GL041467.
 24. Huang, R. J., Seitz, K., Buxmann, J., Hornsby, K. E., Carpenter, L. J., Platt, U., Hoffmann, T.: In situ measurements of molecular iodine in the marine boundary layer: the link to macroalgal species and the implications for O₃, IO, OIO and NO_x, *Atmospheric Chemistry and Physics*, **2010**, 10, 4823-4833.
 25. Ashu-Ayem, E.R., U, Nitschke, C. Monahan, J. Chen, S.B. Darby, P.D. Smith, C.D. O'Dowd, D. B. Stengel, D.S. Venables. Coastal iodine emissions: Part

1. Release of I₂ by *Laminaria digitata* in chamber experiments, submitted, *Environ. Sci. Tech.*, **2012**
26. Gherman, T.; Venables, D. S.; Vaughan, S.; Orphal, J.; Ruth, A. A. Incoherent broadband cavity-enhanced absorption spectroscopy in the near-ultraviolet: application to HONO and NO₂. *Environ. Sci. Technol.* **2008**, 42, 890-895.
27. Chen, J.; Wenger, J. C.; Venables, D. S. Near-ultraviolet absorption cross sections of nitrophenols and their potential influence on tropospheric oxidation capacity. *J. Phys. Chem. A* **2011**, 115, 12235-12242.
28. Spietz, P.; Gómez-Martín, J. C.; Burrows, J. P. Spectroscopic studies of the I₂/O₃ photochemistry Part 2. Improved spectra of iodine oxides and analysis of the IO absorption spectrum. *Photochem. Photobiol. A* **2005**, 176, 50-67.
29. Bloss, W. J.; Rowley, D. M.; Cox, R. A.; Jones, R. L. Kinetics and products of the IO self-reaction. *J. Phys. Chem. A* **2001**, 105, 7840-7854.
30. Derwent, R. G.; Simmonds, P. G.; Manning, A. J.; Spain, T. G., Trends over a 20-year period from 1987 to 2007 in surface ozone at the atmospheric research station, Mace Head, Ireland. *Atmospheric Environment* **2007**, 41, (39), 9091-9098.
31. O'Dowd, C. D.; Geever, M.; Hill, M. K.; Smith, M. H.; Jennings, S. G., New particle formation: Nucleation rates and spatial scales in the clean marine coastal environment. *Geophys. Res. Lett.* **1998**, 25, (10), 1661-1664.

1
2
3
4
5
6
7
8
9
10
11
12
13
14
15
16
17
18
19
20
21
22
23
24
25
26
27
28
29
30
31
32
33
34
35
36
37
38
39
40
41
42
43
44
45
46
47
48
49
50
51
52
53
54
55
56
57
58
59
60

Experiment	I ₂ (ppb _v)	Initial O ₃ (ppb _v)	Max Number Concentration (cm ⁻³)	Mass Flux (μg cm ⁻³ s ⁻¹)	3 nm Max Number Concentration (cm ⁻³)
CH6	1.04	24	2.54×10 ⁶	2.55×10 ⁻⁸	8.88 ×10 ⁴
CH4	1.73	24	5.07×10 ⁶	5.89×10 ⁻⁸	1.77×10 ⁵
CH3	2.88	24	8.66×10 ⁷	1.13×10 ⁻⁶	3.03×10 ⁶
CH2	4.98	24	9.06×10 ⁷	1.20×10 ⁻⁶	3.17×10 ⁶
CH1	6.6	24	6.75×10 ⁷	8.75×10 ⁻⁷	2.36×10 ⁶
CH5	8.1	24	1.05×10 ⁸	2.49×10 ⁻⁶	3.67×10 ⁶

Table 1 Summary of experiments performed with mixing ratios of I₂ and O₃ in a 2200 Litre chamber with a purge flow of 225 L min⁻¹.

1
2
3 **FIGURE 1.** (Top) Typical particle size distribution evolution (Sample #19) over
4 time for *L. Digitata* in chamber without flow-through for low light conditions.
5
6
7
8 (Bottom) Particle concentration, mass flux, I₂ mixing ratio and O₃ mixnign ratio.
9

10
11
12 **FIGURE 2.** Condensation mass flux and particle concentration as a function of I₂
13 mixing ratio. Low, medium and high light-level data are colour coded.
14
15
16
17

18
19
20
21
22 **FIGURE 3.** (Top) Particle size distribution evolution for *L. digitata* (Replicate #25)
23 in chamber without flow-through with low light conditions and an initial mixing ratio
24 of 95.8 ppb_v of O₃. (Bottom) Particle concentration, mass flux and I₂, IO, I₂ and O₃
25 mixing ratios.
26
27
28
29
30

31
32
33
34 **FIGURE 4.** (Top) Aerosol size distribution evolution for laboratory-generated I₂
35 flow-through experiment CH1. (Bottom) Particle concentration, I₂, IO, and O₃
36 mixing ratios for flow-through experiment CH1.
37
38
39
40

41
42
43 **FIGURE 5.** (top) Mass flux and (bottom) particle concentration for low-O₃, static-
44 flow, and moderate-O₃, flow-through, experiments.
45
46
47
48

49
50
51 **FIGURE 6.** Particle concentration as a function of I₂ and CH₂I₂ for this study and
52 previous studies. The mixing ratio range associated with previous studies is shown by
53 horizontal lines on top of graph.
54
55
56
57
58
59
60

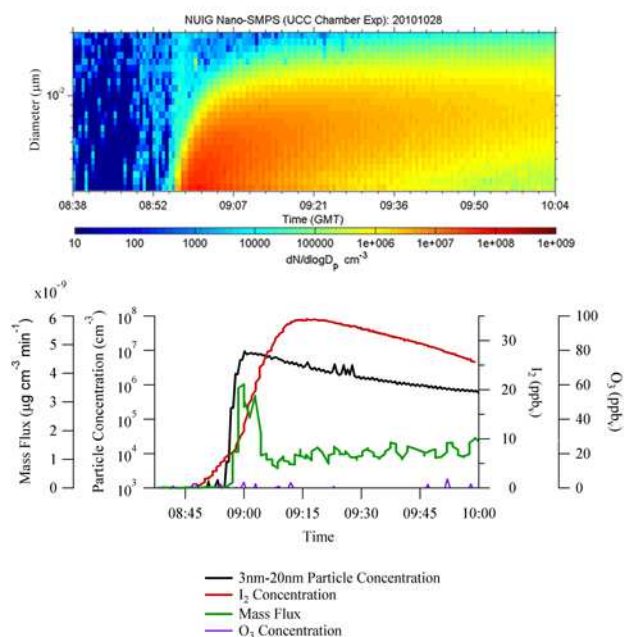


FIGURE 1. (Top) Typical particle size distribution evolution (Sample #19) over time for *L. Digitata* in chamber without flow-through for low light conditions. (Bottom) Particle concentration, mass flux, I₂ mixing ratio and O₃ mixnign ratio.

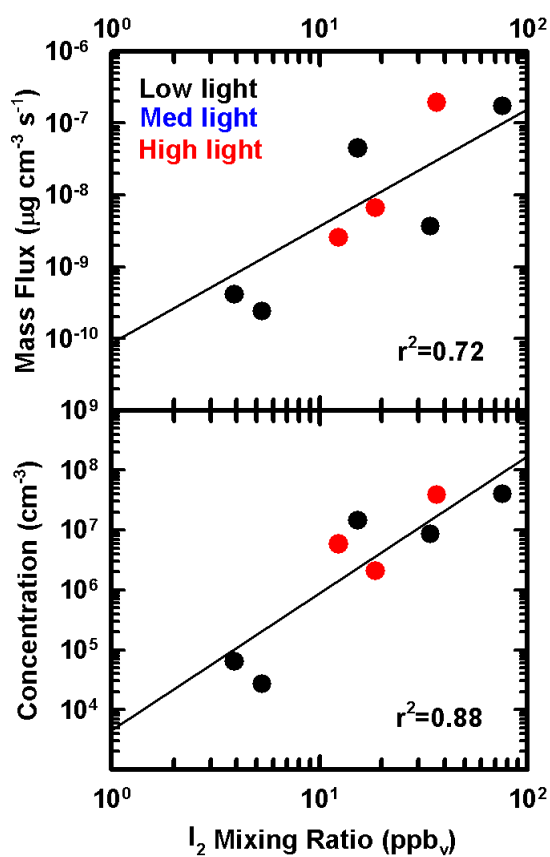


FIGURE 2. Condensation mass flux and particle concentration as a function of I_2 mixing ratio. Low, medium and high light-level data are colour coded.

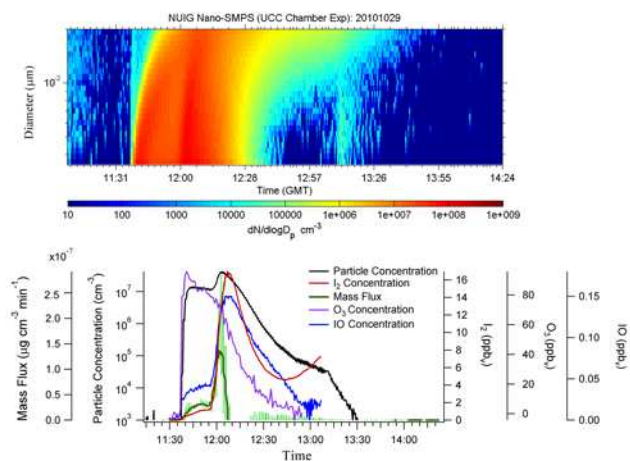


FIGURE 3. (Top) Particle size distribution evolution for *L. digitata* (Replicate #25) in chamber without flow-through with low light conditions and an initial mixing ratio of 95.8 ppb_v of O₃. (Bottom) Particle concentration, mass flux and I₂, IO, I₂ and O₃ mixing ratios.

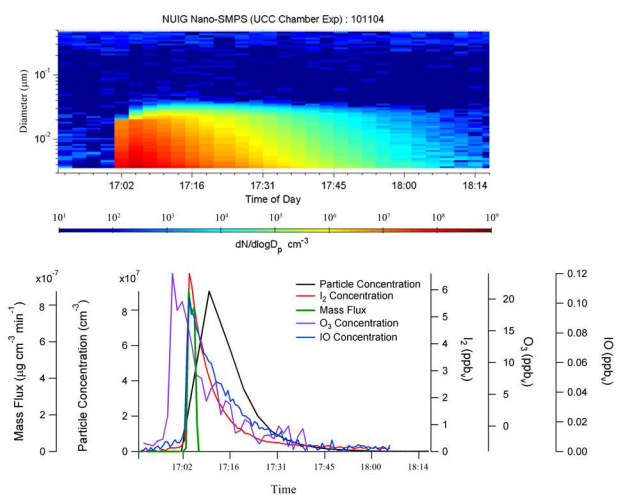


FIGURE 4. (Top) Aerosol size distribution evolution for laboratory-generated I_2 flow-through experiment CH1. (Bottom) Particle concentration, I_2 , IO, and O_3 mixing ratios for flow-through experiment CH1.

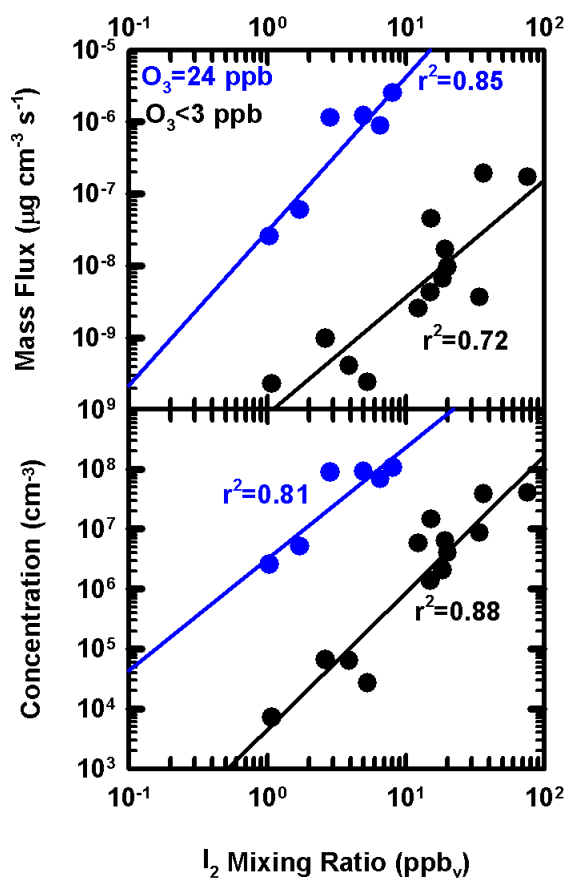


FIGURE 5. (top) Mass flux and (bottom) particle concentration for low- O_3 , static-flow, and moderate- O_3 , flow-through, experiments.

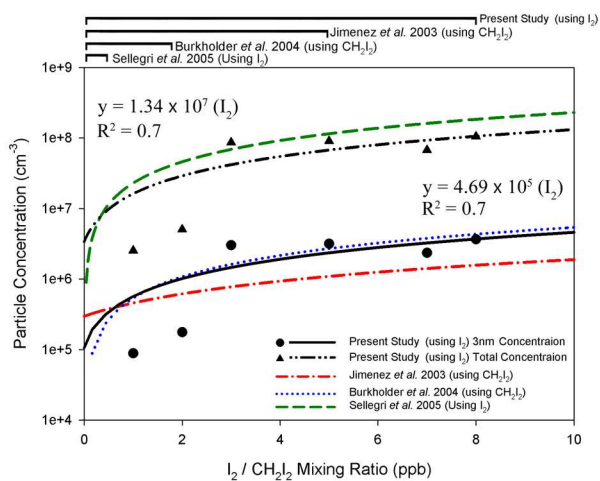


FIGURE 6. Particle concentration as a function of I₂ and CH₂I₂ for this study and previous studies. The mixing ratio range associated with previous studies is shown by horizontal lines on top of graph.

Supplementary Table S1. Laminaria Experiments Summary

Experiment Name	Maximum I ₂ (ppbv)	Max Particle Concentration (cm ⁻³)	Fresh Weight (g)	Dry weight (g)	Max O ₃ (ppb)	Maximum Mass Flux (μg cm ⁻³ s ⁻¹)
With Added Ozone						
#21	0.29	7.9×10 ⁶	274	54	94.6	7.2×10 ⁻⁷
#22	4.23	1.9×10 ⁷	175	35	93.4	8.2×10 ⁻⁸
#23	30.92	2.9×10 ⁷	213	48	95.6	2.0×10 ⁻⁷
#24	23.77	4.2×10 ⁷	185	44	91.5	1.2×10 ⁻⁶
#25	16.96	3.5×10 ⁷	171	35	95.8	2.9×10 ⁻⁷
Low Light						
#16	5.34	2.6×10 ⁴	355	79	-	2.4×10 ⁻¹⁰
#17	3.92	6.3×10 ⁴	238	46	-	4.1×10 ⁻¹⁰
#18	15.39	1.4×10 ⁷	229	54	-	4.4×10 ⁻⁸
#19	34.29	8.5×10 ⁶	676	155	-	3.6×10 ⁻⁹
#20	76.33	3.9×10 ⁷	185	50	-	1.7×10 ⁻⁷
Med Light						
#6	15.22	1.4×10 ⁶	311	48	-	4.2×10 ⁻⁹
#7	20.21	3.9×10 ⁶	380	66	-	9.5×10 ⁻⁹
#8	19.46	6.3×10 ⁶	272	41	-	1.7×10 ⁻⁸
#9	1.09	7.0×10 ³	253	42	-	2.3×10 ⁻¹⁰
#10	2.65	6.5×10 ⁴	03	50	-	9.7×10 ⁻¹⁰
High Light						
#11	12.42	5.7×10 ⁶	360	58	-	2.5×10 ⁻⁹
#12	6.75	1.0×10 ⁷	425	62	-	5.3×10 ⁻⁷
#13	4.05	2.1×10 ⁷	306	44	-	7.2×10 ⁻⁸
#14	18.68	2.1×10 ⁶	330	55	-	6.5×10 ⁻⁹
#15	36.82	3.8×10 ⁷	335	51	-	1.9×10 ⁻⁷

1
2
3
4
5
6
7
8
9
10
11
12
13
14
15
16
17
18
19
20
21
22
23
24
25
26
27
28
29
30
31
32
33
34
35
36
37
38
39
40
41
42
43
44
45
46
47
48
49
50
51
52
53
54
55
56
57
58
59
60